

Scanning tunneling microscopy/spectroscopy on MoS₂ embedded nanowire formed in CVD-grown Mo_{1-x}W_xS₂ alloy

This content has been downloaded from IOPscience. Please scroll down to see the full text.

2017 Jpn. J. Appl. Phys. 56 08LB06

(<http://iopscience.iop.org/1347-4065/56/8S1/08LB06>)

View [the table of contents for this issue](#), or go to the [journal homepage](#) for more

Download details:

IP Address: 130.158.129.94

This content was downloaded on 31/08/2017 at 06:29

Please note that [terms and conditions apply](#).

You may also be interested in:

[Slidable atomic layers in van der Waals heterostructures](#)

Yu Kobayashi, Takashi Taniguchi, Kenji Watanabe et al.

[Inhomogeneous composition distribution in monolayer transition metal dichalcogenide alloys](#)

Shuang Xie, Mingsheng Xu, Shuyun Huang et al.

[NaCl-assisted one-step growth of MoS₂-WS₂ in-plane heterostructures](#)

Zhan Wang, Yong Xie, Haolin Wang et al.

[Controllable growth of monolayer MoS₂ by chemical vapor deposition via close MoO₂ precursor for electrical and optical applications](#)

Yong Xie, Zhan Wang, Yongjie Zhan et al.

[Effect of MoO₃ constituent on the growth of MoS₂ nanosheets by chemical vapor deposition](#)

Xuan Wang, Yong Ping Zhang and Zhi Qian Chen

[The important role of water in growth of monolayer transition metal dichalcogenides](#)

Christoph Kastl, Christopher T Chen, Tevye Kuykendall et al.



Scanning tunneling microscopy/spectroscopy on MoS₂ embedded nanowire formed in CVD-grown Mo_{1-x}W_xS₂ alloy

Hiroyuki Mogi¹, Yu Kobayashi², Atsushi Taninaka¹, Ryuji Sakurada¹, Takahiro Takeuchi¹, Shoji Yoshida¹, Osamu Takeuchi¹, Yasumitsu Miyata², and Hidemi Shigekawa^{1*}

¹Faculty of Pure and Applied Sciences, University of Tsukuba, Tsukuba, Ibaraki 305-8573, Japan

²Department of Physics, Tokyo Metropolitan University, Hachioji, Tokyo 192-0397, Japan

*E-mail: hidemi@ims.tsukuba.ac.jp

Received February 17, 2017; revised May 7, 2017; accepted May 10, 2017; published online July 19, 2017

MoS₂ embedded nanowires formed in a transition-metal dichalcogenide (TMDC) layered semiconductor of Mo_{1-x}W_xS₂ alloy grown by chemical vapor deposition (CVD) on graphite were observed for the first time. Three nanowires radiated outward from the center of each triangular Mo_{1-x}W_xS₂ island to its three corners, suggesting that they were formed during the growth process. The bandgap energy in the wires was 2.38 eV, 0.03 eV narrower than the average bandgap energy in the region surrounding the nanowire. The observed results suggest the possibility of designing embedded nanostructures in a TMDC by controlling the growth conditions, which should lead to further advances in TMDC materials for the development of new types of devices. © 2017 The Japan Society of Applied Physics

1. Introduction

Monolayer transition-metal dichalcogenides (TMDCs), consisting of a transition-metal atomic layer (e.g., W or Mo) sandwiched by two chalcogen atomic layers (S, Se, and Te), have been attracting considerable attention because of their excellent electrical and optical characteristics for applications.^{1–9} They are chemically stable and their bandgap energy varies in the visible-light range (for example, MoS₂: 2.4 eV,¹⁰ WS₂: 2.7 eV¹¹). To increase the applicability of their characteristics, tunability of the bandgap energy is a key factor and strongly desired. Recently, this requirement has been realized by the growth of Mo_{1-x}W_xS₂ and Mo_{1-x}W_xSe₂ alloys, for which the bandgap energy has been confirmed to be tunable via their compositional ratios.^{12–15} The formation of heterostructures using these alloys has enabled tunable band alignment.^{16–18}

For the further development of these promising materials, the fabrication of nanostructures is the next target. For III–V and other compound semiconductors, metal organic chemical vapor deposition (MOCVD) and molecular beam epitaxy (MBE) are well-established growth methods for producing highly functional devices based on the fabrication of quantum structures such as quantum wells, quantum wires, and quantum dots.^{19–21} To utilize such characteristics of alloys in TMDCs, a deeper understanding of their growth mechanism is urgently required. Here we present the results of a scanning tunneling microscopy/spectroscopy (STM/STS) study on the growth process of Mo_{1-x}W_xS₂, in which the formation of MoS₂ embedded nanowires was observed for the first time.

2. Sample preparation

Figure 1 shows a schematic illustration of the sample preparation. Mo_{1-x}W_xS₂ was formed on kish graphite (Covalent Materials) by high-temperature CVD.²² The graphite was mechanically exfoliated onto a quartz substrate using Nitto tape (SPV-224). The substrate was placed in a quartz tube (3 cm diameter, 100 cm length) with WO₃ powder (Aldrich, 99% purity, 100 mg), MoO₃ powder (Aldrich, 99% purity, 0.2 mg), and sulfur flakes (Aldrich, 99.99% purity, 2 g). The quartz tube was then filled with Ar gas at a flow rate

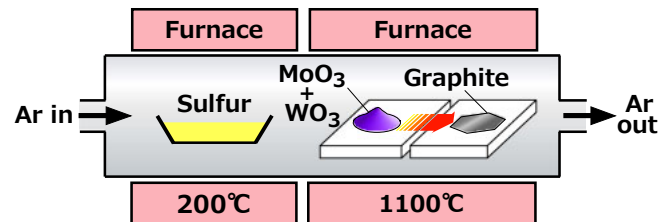


Fig. 1. (Color online) Schematic illustration of the growth process of Mo_{1-x}W_xS₂ on graphite by CVD with an Ar gas flow.

of 100 cm³/min. The temperature of the substrate and the WO₃ and MoO₃ was gradually increased to the growth temperature (1100 °C) over 60 min using an electrical furnace. When the substrate temperature reached the set value, the sulfur was heated at 200 °C for 15–30 min using another electrical furnace to supply sulfur vapor to the substrate. After the growth, the quartz tube was immediately cooled using an electric fan.

3. Characterization of the sample

First, compositional analysis was carried out using Raman spectroscopy (RS). Figure 2 shows secondary electron microscope (SEM; acceleration energy of 0.8 keV) images of Mo_{1-x}W_xS₂ alloy samples formed on kish graphite and the Raman spectra obtained from a triangular island. The shape of the islands depends on the Mo+W : S ratio in the vapor and the temperature,²³ and equilateral triangular islands with threefold symmetry of the lattice were grown under the present conditions. Multilayered islands were brightly imaged and the dark area outside the islands corresponds to the graphite substrate. As shown in Fig. 2(b), the island comprises a small equilateral triangle surrounded by a slightly larger one. As previously studied, the inner equilateral triangular area is not a second layer but an area of Mo-rich Mo_{1-x}W_xS₂ alloy surrounded by an area of W-rich alloy corresponding to the larger triangle, i.e., a heterostructure of W-rich and Mo-rich Mo_{1-x}W_xS₂ alloys is formed.^{14,16} As indicated in Fig. 2(b), a rodlike nucleus existed near the center of each Mo-rich area.

Figures 2(c) and 2(d) show Raman spectra obtained for the pure MoS₂ and WS₂, and Mo_{1-x}W_xS₂ alloy formed on

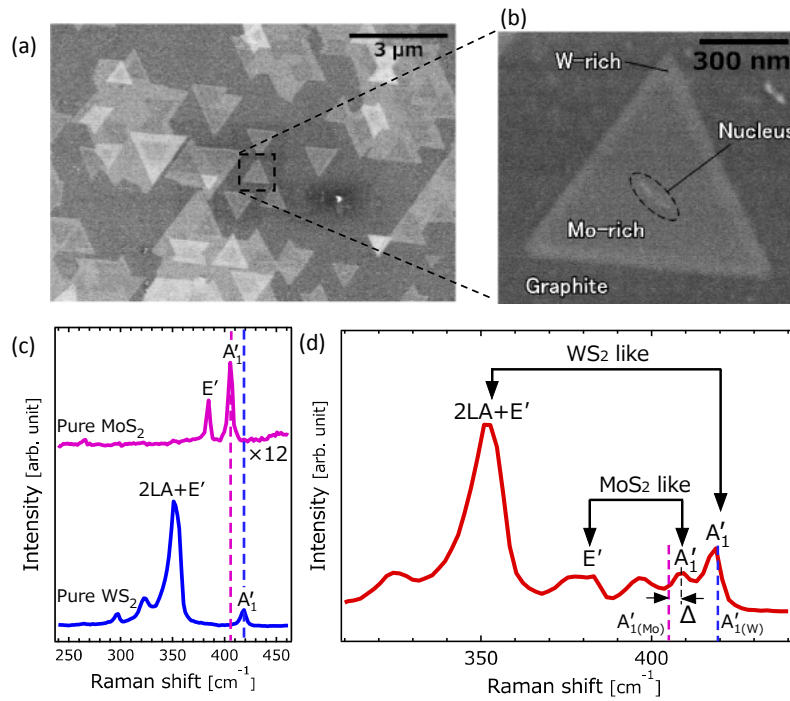


Fig. 2. (Color online) (a) SEM image of $\text{Mo}_{1-x}\text{W}_x\text{S}_2$ grown on graphite. (b) Magnification of a triangular $\text{Mo}_{1-x}\text{W}_x\text{S}_2$ island in the square in (a). (c) Raman spectra obtained for pure MoS_2 and WS_2 formed on graphite. (d) Raman spectrum obtained from $\text{Mo}_{1-x}\text{W}_x\text{S}_2$ grown on graphite. From the shift of the Raman peaks in the spectrum from those for the pure MoS_2 and WS_2 in (c), the component ratio x was estimated to be 0.3 and 0.9 for Mo-rich and W-rich areas, respectively.

graphite, respectively. The sample was excited by a laser with a wavelength of 532 nm and spot size of 1 μm at room temperature. The peaks for the pure MoS_2 (405 cm^{-1}) and WS_2 (419 cm^{-1}) are assigned to A_{1g} in Fig. 2(c),²²⁾ and it has been reported that the Raman spectra of monolayer $\text{Mo}_{1-x}\text{W}_x\text{S}_2$ alloys exhibit three characteristic peaks in the region from 350 to 420 cm^{-1} , which are assigned to the WS_2 -like E' , MoS_2 -like E' , and A'_1 modes in order of increasing frequency. The frequency of the A'_1 mode increases almost linearly with increasing W concentration from the value for the A'_1 mode of pure MoS_2 to that for WS_2 .^{12,14,24)} Therefore, from the observed positions of A'_1 for the MoS_2 -like (409 cm^{-1}) and WS_2 -like (419 cm^{-1}) peaks, the component ratio of x was estimated to be 0.3 (Mo-rich area) and 0.9 (W-rich area), respectively, where the value of 0.3 is in good agreement with that obtained in our previous paper.¹⁶⁾

4. STM/STS analysis

Figure 3(a) shows an STM image of a $\text{Mo}_{1-x}\text{W}_x\text{S}_2$ heterostructure formed on graphite. A Mo-rich triangular structure is surrounded by a W-rich area. As shown by the cross section in Fig. 3(b), the heights of the islands are ~ 0.6 and $\sim 0.8\text{ nm}$ for the W-rich and Mo-rich areas, respectively, which are in good agreement with the height of a monolayer of $\text{Mo}_{1-x}\text{W}_x\text{S}_2$ (0.6 nm). The observed difference of 0.2 nm for the Mo-rich area originates from the higher local density of states (LDOS) in this area. As shown in the previous paper, we counted Mo and W atoms using high-resolution STM images of the same sample.¹⁶⁾ The average Mo : W ratios were 1 : 9 for a W-rich area and 7 : 3 for a Mo-rich area in good agreement with the results obtained by Raman measurement in this work.

As shown in Figs. 3(c) and 3(d), three wires with nanoscale width radiated outward from the nucleus in the triangular

island to its three corners, as schematically shown in the inset of Fig. 3(d) and in Fig. 3(e). These characteristics were observed for all the islands. Figure 4(a) shows an STM image of a nanowire including its surrounding area. As described above, the average Mo : W ratio in the Mo-rich area was 7 : 3 according to the result of Raman measurement (averaged over an area of $\sim 1\text{ }\mu\text{m}^2$). As shown in Fig. 4(a), however, there are nanoscale domains with different brightnesses in the area surrounding the nanowire, which correspond to $\text{Mo}_{1-x}\text{W}_x\text{S}_2$ areas with different values of x , namely, the alloy was not uniformly formed at the nanoscale. Figure 4(b) shows a high-resolution image of a nanowire, in which each atom in the nanowire is clearly imaged. Since Mo and W atoms are respectively imaged as bright and dark areas in $\text{Mo}_{1-x}\text{W}_x\text{S}_2$ alloy,¹⁶⁾ the central area in the nanowire, where all atoms are imaged as bright areas, is considered to be pure MoS_2 . As shown in our previous paper, the electronic structure of a Mo-rich/W-rich area is strongly influenced by the Mo/W composition in the surrounding areas,¹⁶⁾ which is considered to produce the variation in the brightness in the nanowire. In fact, the wide part of the nanowire, which is surrounded by a larger Mo-rich area, is observed to be brighter.

These nanowires are considered to show the growth trajectory of the corner of the island. Namely, the Mo-rich area is grown from both ends of the nucleus. Since the growth nucleus has a rod shape, the starting point of nanowire growth is not located at the center of the Mo-rich area. However, since a metal-terminated edge (Mo or W) is stable, the island becomes an equilateral triangle, which is the structure of TMDC schematically shown in Fig. 5.^{23,25)}

Figure 4(c) shows spectra obtained from above the central area of a nanowire (red) and those averaged over the area surrounding the nanowire in the Mo-rich area (blue). These spectra were obtained by averaging 500 spectra in each area.

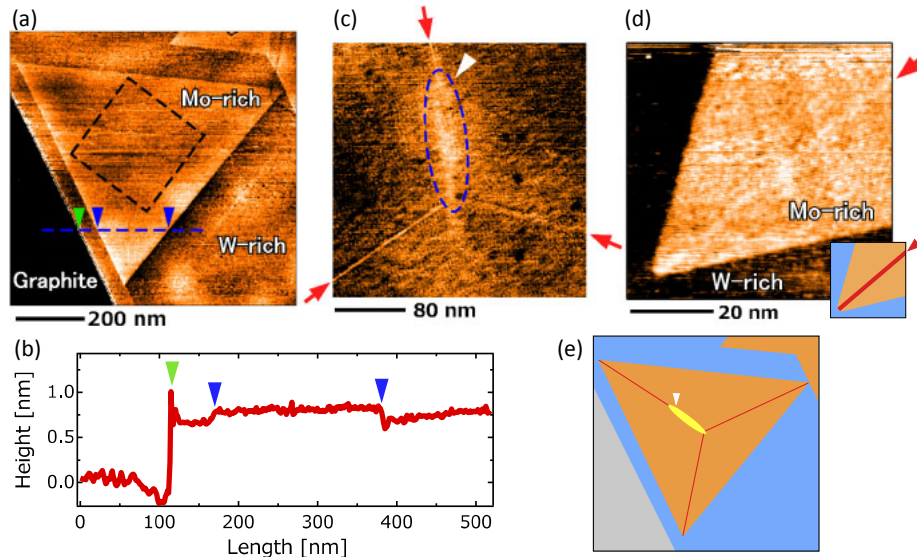


Fig. 3. (Color online) (a) STM image of a $\text{Mo}_{1-x}\text{W}_x\text{S}_2$ heterostructure formed on a graphite in a Mo-rich triangle area surrounded by a W-rich area (sample bias $V_s = 1.4$ V, setpoint tunnel current $I_t = 80$ pA). (b) Cross section obtained along the line in (a). (c) and (d) magnifications of the center and a corner of the Mo-rich triangular island in (a), respectively ($V_s = 1.6$ V, $I_t = 200$ pA, 80 K). The inset in (d) shows a schematic view of the structure. Red arrows mark the positions of nanowires. The nucleus is enclosed within a blue dashed ellipse. (e) Composition-emphasized schematic model of the same area as in (a). Red lines represent the nanowires shown in (c) and (d). The white arrow corresponds to that shown in (c).

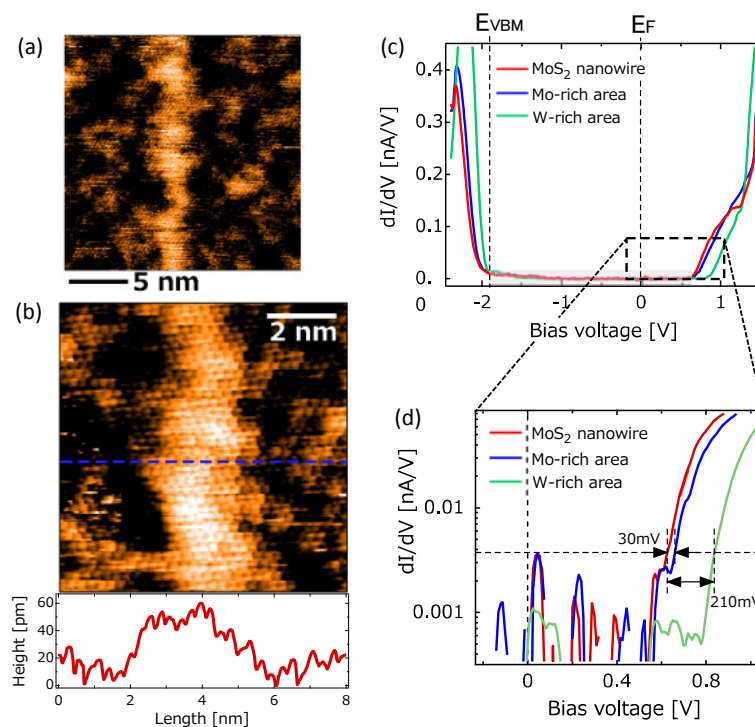


Fig. 4. (Color online) (a) Wide-range STM image of a MoS_2 wire formed in a Mo-rich area ($V_s = 0.7$ V, $I_t = 100$ pA). (b) High-resolution image of a MoS_2 wire and the cross section along the blue line in the image ($V_s = 1.5$ V, $I_t = 300$ pA, 80 K). (c) Spectra obtained from above a MoS_2 wire and the surrounding area (Mo-rich area). A spectrum obtained over a W-rich area is also shown for comparison. (d) Enlargement of part of (c) showing the conduction band edge. The horizontal dashed line indicates the threshold where the effective signal is higher than the noise level.

For comparison, a spectrum obtained in the W-rich area is also shown (green), for which the bandgap energy was 2.73 eV and close to the value for pure WS_2 (2.74 eV). Since the bandgap energy markedly changes with the shift of the conduction band edge in the Mo-rich area,¹⁶ a magnification of the conduction band edge is shown in a logarithmic plot in Fig. 4(d) to show the shift clearly. The bandgap energy in the wires was about 2.38 eV, close to the value for pure MoS_2

(2.4 eV) as expected, and 0.03 eV less than the bandgap energy averaged over the region surrounding the nanowire. Here, the conduction band edge E_{CBM} and the valence band edge E_{VBM} were determined using the bias voltages at which the signal became higher than the noise level. The difference in the bandgap is less than that obtained in our previous paper, 0.075 eV, because measurement was carried out in Mo and W areas in $\text{Mo}_{1-x}\text{W}_x\text{S}_2$ in the previous paper. To obtain a

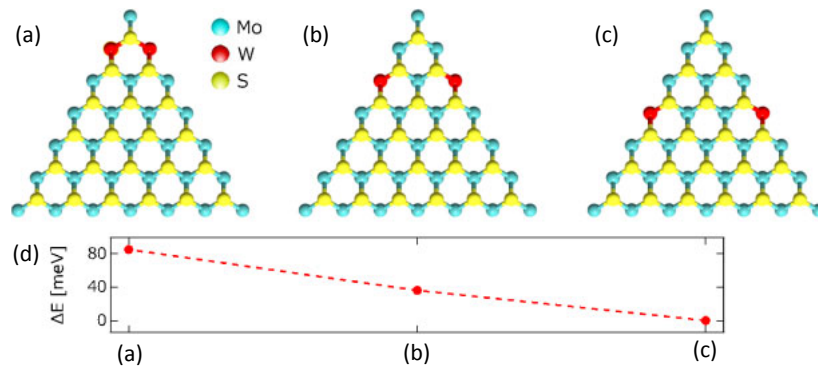


Fig. 5. (Color online) (a–c) Three structures used for simulation. (d) Relative change in the total energy.

larger shift in the bandgap energy to make the nanowire more applicable, a larger value of x such as 0.9 is required.²⁶⁾

5. Simulation

To determine the mechanism of the nanowire growth process in more detail, a simple simulation was carried out. Figures 5(a)–5(c) show the schematic structures used for the simulation. A pair of Mo atoms in a triangular MoS₂ structure were replaced by two W atoms, as indicated by two red circles in each diagram. The simulation was carried out using Atomistix ToolKit with the Perdew–Burke–Ernzerhof (PBE) exchange interaction potential for the generalized gradient approximation (GGA).²⁷⁾ A double- ζ base was used for all atoms and the cutoff energy was set to 100 Ry. The relative difference in the total energy with the change in the position of W atoms is shown in Fig. 5(d). The fact that the total energy decreases as the structure changes from (a) to (c) suggests the preferential adsorption of W atoms at the edges away from the corner of the triangular MoS₂ crystal. The distance moved by W atoms is considered to depend on the growth conditions, such as the temperature and the composition of the Mo/W vapor. This could lead to the formation of a MoS₂ wire with a certain width (about 3 nm in this experiment) during the growth of Mo_{1-x}W_xS₂ alloy. More detailed simulations using molecular dynamics, for example, with a more realistic size are necessary to obtain further understanding of the formation of a MoS₂ wire.

6. Summary

MoS₂ embedded nanowires formed in a transition-metal dichalcogenide (TMDC) layered semiconductor of Mo_{1-x}W_xS₂ alloy during its growth by chemical vapor deposition (CVD) on graphite were observed for the first time. The bandgap energy in the wires was about 2.38 eV, 0.03 eV narrower than the average bandgap energy in the region surrounding the nanowire. The observed results suggest the possibility of designing nanostructures in a TMDC by controlling the growth conditions, which should lead to the development of new types of devices.

Acknowledgements

This work was supported by Japan Society for the Promotion of Science in the form of Grants-in-Aid for Scientific Research (15H05734 and 16H00918) and CREST, Japan Science and Technology Agency.

- 1) A. Splendiani, L. Sun, Y. Zhang, T. Li, J. Kim, C. Y. Chim, G. Galli, and F. Wang, *Nano Lett.* **10**, 1271 (2010).
- 2) B. Radisavljevic, A. Radenovic, J. Brivio, V. Giacometti, and A. Kis, *Nat. Nanotechnol.* **6**, 147 (2011).
- 3) M. Bernardi, M. Palumbo, and J. C. Grossman, *Nano Lett.* **13**, 3664 (2013).
- 4) Y. Yu, S. Hu, L. Su, L. Huang, Y. Liu, Z. Jin, A. A. Purezky, D. B. Geohegan, K. W. Kim, Y. Zhang, and L. Cao, *Nano Lett.* **15**, 486 (2015).
- 5) D. Kozawa, R. Kumar, A. Carvalho, K. K. Amara, W. Zhao, S. Wang, M. Toh, R. M. Ribeiro, A. H. C. Neto, K. Matsuda, and G. Eda, *Nat. Commun.* **5**, 4543 (2014).
- 6) K. F. Mak, C. Lee, J. Hone, J. Shan, and T. F. Heinz, *Phys. Rev. Lett.* **105**, 136805 (2010).
- 7) K. F. Mak, K. L. McGill, J. Park, and P. L. McEuen, *Science* **344**, 1489 (2014).
- 8) D. Jariwala, V. K. Sangwan, L. J. Lauhon, T. J. Marks, and M. C. Hersam, *ACS Nano* **8**, 1102 (2014).
- 9) Y. Kobayashi, S. Yoshida, R. Sakurada, K. Takashima, T. Yamamoto, T. Saito, S. Konabe, T. Taniguchi, K. Watanabe, Y. Maniwa, O. Takeuchi, H. Shigekawa, and Y. Miyata, *Sci. Rep.* **6**, 31223 (2016).
- 10) Y. L. Huang, Y. Chen, W. Zhang, S. Y. Quek, C.-H. Chen, L. J. Li, W. T. Hsu, W.-H. Chang, Y. J. Zheng, W. Chen, and A. T. S. Wee, *Nat. Commun.* **6**, 6298 (2015).
- 11) B. Zhu, X. Chen, and X. Cui, *Sci. Rep.* **5**, 9218 (2015).
- 12) Y. Chen, J. Xi, D. O. Dumcenco, Z. Liu, K. Suenaga, D. Wang, Z. Shuai, Y. S. Huang, and L. Xie, *ACS Nano* **7**, 4610 (2013).
- 13) D. O. Dumcenco, H. Kobayashi, Z. Liu, Y. S. Huang, and K. Suenaga, *Nat. Commun.* **4**, 1351 (2013).
- 14) Y. Kobayashi, S. Mori, Y. Maniwa, and Y. Miyata, *Nano Res.* **8**, 3261 (2015).
- 15) S. Tongay, D. S. Narang, J. Kang, W. Fan, C. Ko, A. V. Luce, K. X. Wang, J. Suh, K. D. Patel, V. M. Pathak, J. Li, and J. Wu, *Appl. Phys. Lett.* **104**, 012101 (2014).
- 16) S. Yoshida, Y. Kobayashi, R. Sakurada, S. Mori, Y. Miyata, H. Mogi, T. Koyama, O. Takeuchi, and H. Shigekawa, *Sci. Rep.* **5**, 14808 (2015).
- 17) S. Zheng, L. Sun, T. Yin, A. M. Dubrovkin, F. Liu, Z. Liu, Z. X. Shen, and H. J. Fan, *Appl. Phys. Lett.* **106**, 063113 (2015).
- 18) K. Bogaert, S. Liu, J. Chesin, D. Titow, S. Gradečak, and S. Garaj, *Nano Lett.* **16**, 5129 (2016).
- 19) L. L. Chang, L. Esaki, and R. Tsu, *Appl. Phys. Lett.* **24**, 593 (1974).
- 20) J. P. van der Ziel, R. Dingle, R. C. Miller, W. Wiegmann, and W. A. Nordland, *Appl. Phys. Lett.* **26**, 463 (1975).
- 21) B. Ketterer, A. V. Kuhlmann, J. Houel, and J. R. Morante, *Nat. Mater.* **12**, 439 (2013).
- 22) Y. Kobayashi, S. Sasaki, S. Mori, H. Hibino, Z. Liu, K. Watanabe, T. Taniguchi, K. Suenaga, Y. Maniwa, and Y. Miyata, *ACS Nano* **9**, 4056 (2015).
- 23) S. S. Wang, Y. M. Rong, Y. Fan, M. Pacios, H. Bhaskaran, K. He, and J. H. Warner, *Chem. Mater.* **26**, 6371 (2014).
- 24) Y. Chen, D. O. Dumcenco, Y. Zhu, X. Zhang, N. Mao, Q. Feng, M. Zhang, J. Suh, P. H. Tan, Y. S. Huang, and L. Xie, *Nanoscale* **6**, 2833 (2014).
- 25) A. M. van der Zande, P. Y. Huang, D. A. Chenet, T. C. Berkelbach, Y. You, G. H. Lee, T. F. Heinz, D. R. Reichman, D. A. Muller, and J. C. Hone, *Nat. Mater.* **12**, 554 (2013).
- 26) J. Kang, H. Sahin, and F. M. Peeters, *J. Phys. Chem. C* **119**, 9580 (2015).
- 27) J. P. Perdew, K. Burke, and M. Ernzerhof, *Phys. Rev. Lett.* **77**, 3865 (1996).